Available online at www.sciencedirect.com
SCIENCE DIRECT
Journal of Power Sources 157 (2006) 799–808
JOURNAL OF POWER SOURCES
www.elsevier.com/locate/jpowsour

Experimental assessment of energy-management strategies in fuel-cell propulsion systems

P. Corbo *, F.E. Corcione, F. Migliardini, O. Veneri

Istituto Motori, Italian National Research Council, Via G. Marconi, 8, 80125 Napoli, Italy

Received 29 September 2005; accepted 2 January 2006
Available online 14 February 2006

Abstract

The limitations of electric vehicles equipped with electrochemical batteries justify strong research interest for new solutions, based on hydrogen fuel-cell technology that are able to improve vehicle range, and reduce battery recharging time, while maintaining the crucial advantages of high efficiency and local zero emissions. The best working of a fuel-cell propulsion system, in terms of optimum efficiency and performance, is based on specific strategies of energy management, that are designed to regulate the power flows between the fuel cells, electric energy-storage systems and electric drive during the vehicle mission. An experimental study has been carried out on a small-size electric propulsion system based on a 2.5-kW proton exchange membrane fuel cell stack and a 2.5-kW electric drive. The fuel-cell system has been integrated into a powertrain comprising a dc–dc converter, a lead–acid battery pack, and brushless electric drive. The experiments are conducted on a test bench that is able to simulate the vehicle behaviour and road characteristics on specific driving cycles. The experimental runs are carried out on the European R40 driving cycle using different energy-management procedures and both dynamic performance and energy consumption are evaluated.

Keywords: Proton exchange membrane; Fuel cell; Power train; Electric vehicles; Energy management; Driving cycle

1. Introduction

It is well known that the current world energy market is mainly based on oil (about 65%), with obvious implications as regard pollution and geo-political issues. On the other hand, the legitimate aspiration of developing nations to reach life conditions comparable with those of industrialized countries and the continuous growth of world population are the main causes of the increase in energy demand and of the associated increase in greenhouse gas emissions. In order to face this challenge, two main approach have to be adopted, namely, an increase in energy-conversion efficiency and a reduction of hydrocarbon utilization. To this end, the use of an alternative energy carrier, such as hydrogen, assumes a fundamental role in all the fields of energy utilization, including the transportation sector.

Although improvements in conventional engine technologies have partially mitigated the above problems, and further refinements could provide additional progress (e.g., hybrid gasoline-electric vehicles), fuel-cell vehicles (FCVs) appear to be a promising means of transportation that is capable of using hydrogen as a fuel In fact, FCVs would overcome the typical limitations of electric vehicles equipped with traditional energy-storage systems (driving range, battery weight and recharging time) and could become a primary vehicle technology that is characterized by high efficiency and no pollutant emission [1–4].

Proton exchange membrane fuel cells (PEMFCs) are the most likely candidates for automotive applications, due to their high power density and low operative temperature (60–90 °C), with consequent fast start-up, good dynamic behaviour and reliable service if fuelled by pure hydrogen [5,6]. The only product of the electrochemical reaction of hydrogen oxidation is water, and typical stack efficiencies are higher than 55%. Because of their tolerance to carbon dioxide and the possibility to use air as an oxidant, the PEMFC is preferred to other types of fuel cell operating at low-temperature e.g., alkaline electrolyte (AFC). PEMFC requires several auxiliary components for its operation, in particular an air compressor for oxidant supply, and thermal- and water- management systems for membrane humidification and stack temperature control. The energy required by these auxiliaries, particularly by the air compressor, can be significant

* Corresponding author. Tel.: +39 081 7177180; fax: +39 081 2396097.
E-mail address: p.corbo@im.cnr.it (P. Corbo).

0378-7753/$ – see front matter © 2006 Elsevier B.V. All rights reserved.
doi:10.1016/j.jpowsour.2006.01.004

and there by limit the overall efficiency of the fuel-cell system [7].

The development of FCVs requires on-board integration of the fuel-cell systems and electric energy-storage devices with appropriate energy management, and then the different hybridization levels between the storage and on-board generation systems have to be effected in real driving conditions in order to assess the prospects of these propulsion systems in terms of performance and efficiency.

This paper reports the experimental results obtained from a fuel-cell propulsion system that is installed on a laboratory test bench. It utilizes a 2.5-kW PEMFC stack, a 2.5-kW maximum power electrical drive and a lead–acid battery pack as a storage system. The goal is to study the dynamic behaviour of the fuel-cell system on the European R40 driving cycle, and to obtain information about the effect of different energy-management strategies on powertrain efficiency.

2. Experimental

The laboratory experimental activity was carried out on a complete powertrain that was comprised of a fuel-cell system, a dc–dc converter, an electrical energy-storage system, an electrical drive, and data–acquisition systems. The propulsion system was coupled to a braking electrical machine that was able to effect different driving cycles by purpose designed control software. The technical characteristics of the above components have been reported and discussed in a previous paper [7], except for the electrical drive whose rated power was changed for the experiments reported here. The main data of all components are summarized in Table 1, while a scheme of the overall apparatus is given Fig. 1.

The fuel-cell system (FCS), realized by PROTON MOTOR Fuel Cell GmbH, was based on a 2.5-kW PEMFC stack that was fuelled with compressed pure hydrogen. The stack worked at low pressure (25–40 kPa, dead-end operation), and was equipped with all the auxiliary components that were necessary to the fuel-cell operation, such as air supply unit; fuel supply unit, cooling system, humidification system, and fuel-cell control system. A LAFERT brushless engine of 2.5-kW maximum power, of the

Table 1
Technical specifications of overall powertrain

Proton motor fuel-cell system (FCS)	
Electric output	Max 2 kW after dc–dc converter
Dynamic	Max change rate 500 W s^{-1}
Hydrogen	Purity of 99.999% H_2 FCS inlet gas pressure: 500 kPa FCS inlet gas stream: at least 3 Nm^3 h^{-1}
Nitrogen	Purity of 99.999% N_2 FCS inlet gas pressure: 500 kPa FCS inlet gas stream at least 1 Nm^3 h^{-1}
Max stack temperature (K)	<343
Communication	Ethernet/TCP IP
Max cooling water in (K)	333
Small battery max power output 12 V (A)	10
Small battery max recharging current (A)	4
Air compressor	Side channel, 24VDC, max pressure 16 kPa
Water pump (cooling and humidification)	Circulating pump, 24 V dc, 20 kPa, 7 l min^{-1}
Electrical drive	
Type	Brushless
Maximum power (kW)	2.5
Rated current (A)	32
Maximum current (A)	100
Link voltage (V)	48
Motor voltage (V)	35
2p	4
Rated speed (rpm)	3000
Maximum speed (rpm)	6000
dc–dc converter	
Maximum inlet voltage (V)	34
Minimum inlet voltage (V)	19
Rated inlet voltage (V)	24
Rated output voltage (V)	48 ± 1%
Rated power (kW)	2.8
Rated efficiency (%)	86
Traction batteries (lead acid)	
Voltage (V)	12
Capacity (Ah)	38

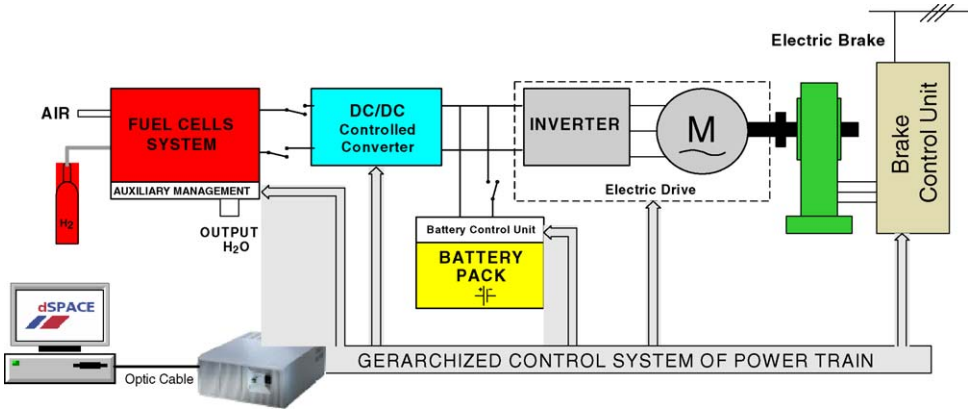

Fig. 1. Scheme of fuel-cell powertrain.

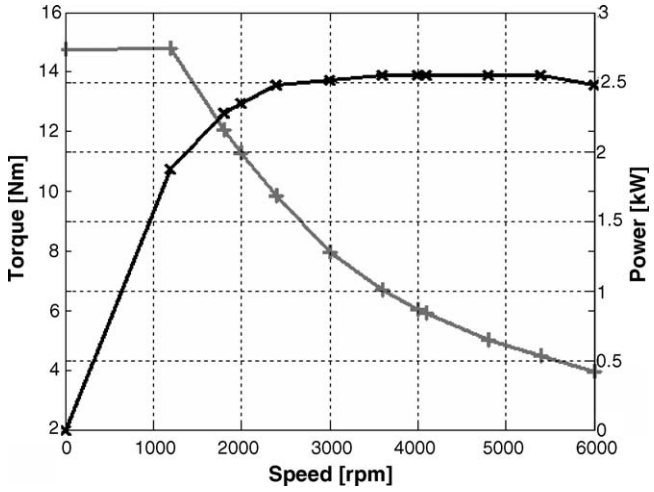

Fig. 2. Characteristic curves of electric engine.

same type that is installed in electrical commercial mopeds and equipped with a controlled inverter, was used. Its characteristic curves are reported in Fig. 2 in terms of power and torque versus revolution speed. A lead–acid battery pack of four units, each of 12 V and 38 Ah, was used as electrical energy-storage system.

The stack output voltage ranged from 34 V at open-circuit to 22 V at full load, while the electrical engine required electric current at 48 V dc, then a dc–dc converter was necessary to match the stack output voltage to that required by the engine. This is a critical component in the energy-flow management within the propulsion system, in particular it allows the stack output power to be controlled according to the selected strategy. This control was performed by automatic regulation of current at the device output, depending on the power required by the driving cycle. Downstream of the converter, a dc bus permitted the connection between converter, battery pack and electric load. LEM voltage and current sensors were installed on batteries, and upstream-downstream on the dc–dc converter to monitor the electric energy flows between the different components of the propulsion system. The energy flow was unidirectional from the stack toward the d.c. bus, while the battery pack could be recharged by both the stack and the engine during regenerative braking [8] and discharged when the energy required from the engine was higher than the energy provided by the fuel-cell system. A I/O laboratory board was used for data-acquisition and control of the electrical parameters the effect the dc–dc converter behaviour.

The control scheme utilized for the automatic execution of the dynamic cycles is shown in Fig. 3. In order to effect different driving cycles the engine was coupled to an eddy current braking machine that was controlled by a specific software. Since, the engine-to-wheel speed ratio fixed, it was possible to reproduce vehicle inertia by means of an equivalent flywheel, while aerodynamic drag and rolling resistance were performed by the eddy current brake. A speed PID controller was adopted to simulate the automatic pilot, while a torque PID controller was used to simulate both the aerodynamic drag and the rolling resistance of the vehicle. The PID controllers were programmed and calibrated in Lab View and were integrated in the overall software that was utilized to control the braking machine during the driving cycles. Finally, some security switches were adopted in order to disconnect instantaneously the electric load from battery pack and/or stack.

3. Results and discussion

Details of the fuel-cell system characterization are reported in [7], where the energy losses associated with the individual sub-systems were determined. The stack and overall system efficiencies, reported in Fig. 4, were calculated by the following equations:

$$\text{Stack efficiency} : \eta_{\text{stack}} = \frac{V}{V_{\text{id}}} \tag{1}$$

where V is the measured output stack voltage and V_{id} is the reversible open-circuit slack voltage (1.23 V for each cell), given by $-\Delta G_{\text{f}}/2\text{F}$. Here ΔG_{f} is the Gibbs free energy of formation in the normal state for the reaction $H_2 + 1/2O_2 = H_2O$, while F is the Faraday constant. The total efficiency of the fuel-cell system is given by:

$$\eta_{\text{FCS}} = \frac{P_{\text{IN}_{\text{DC}}}}{P_{\text{H}_2}} \tag{2}$$

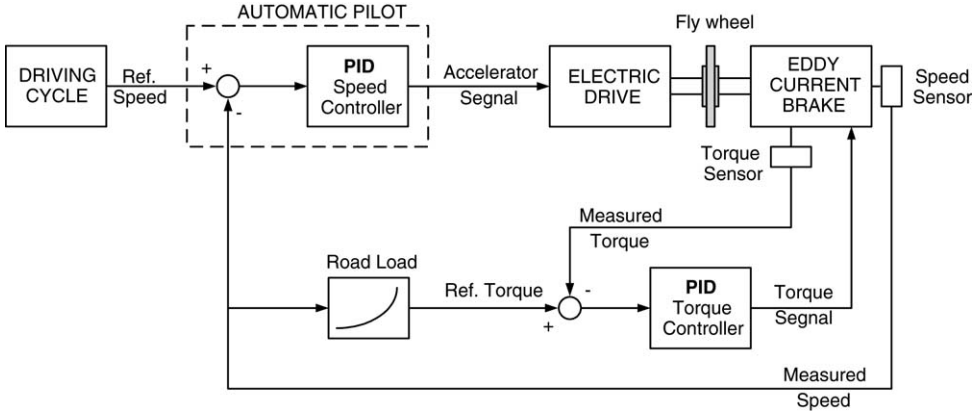

Fig. 3. Control scheme of automatic execution of dynamic cycles.

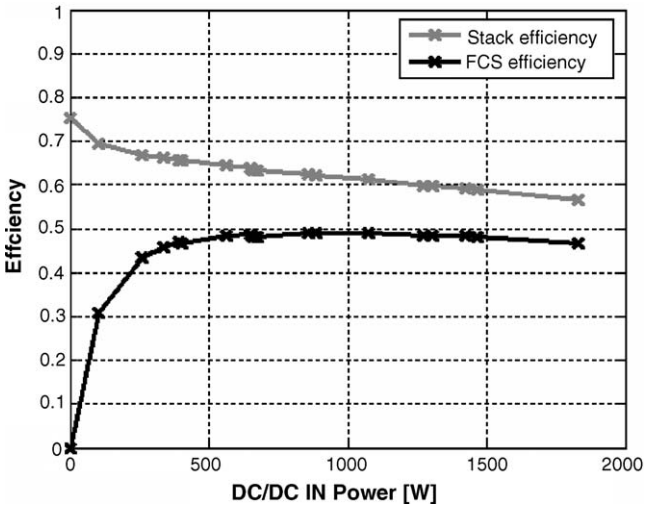

Fig. 4. Stack and fuel-cell system efficiency vs. dc–dc converter inlet power. Experimental conditions: $R = 2$–6, $T = 60\,^{\circ}\mathrm{C}$, $P_{H_2} < 50$ kpa, $P_{air} < 20$ kPa.

which expresses the ratio between the power at the dc–dc converter input and the theoretical power associated with the fuel entering the stack. In Eq. (2), P_{H_2} is calculated from:

$$P_{H_2} = \frac{P_{stack}}{\eta_{therm}\eta_{util}\eta_{stack}} \quad (3)$$

where P_{stack} is the power supplied by the stack; η_{therm} is the thermodynamic efficiency defined by the ratio of ΔG_f to ΔH_f, which is the lower heating value for hydrogen combustion (0.98 at 298 K); η_{util} is the fuel utilization efficiency defined as ratio between mass of fuel reacted in the stack and mass of fuel entering the stack. The value of η_{util} was experimentally estimated from the opening time of the anode purge valve and the opening frequency and purged volume; found to be 0.98.

The data in Fig. 4 show that, in spite of different causes of energy loss inside the system, the FCS global efficiency is about 50% over a wide range of loads. The major energy consumption is due to the air compressor (about 120 W at 1.8 FCS power), while minor losses are associated with the cooling and humidification water pumps (about 10 W for each, constant with respect to load). Further consumptions are due to the different electrical devices present inside the system, such as cables, sensors, electric valves, relays, and control system boards.

The experimental tests on the overall powertrain were performed with the main goal of evaluating the total efficiency using different energy-management strategies and verifying the stack behaviour during dynamic phases, including start-up. This was carried by testing the engine on the R40 European urban driving cycle. This cycle (Fig. 5) is composed by three phases: the first two are characterized by acceleration, constant speed (1500 and 3200 rpm) and deceleration steps, while the third phase presents two steps at constant speed (5000 and 3500 rpm), before returning to zero speed. For all tests discussed in this paper, the energy contribution of the fuel cell system was regulated by maintaining the voltage reference value at the dc–dc converter output so that it was higher than the maximum battery recharging voltage to allow the energy flow to be always directed towards the load

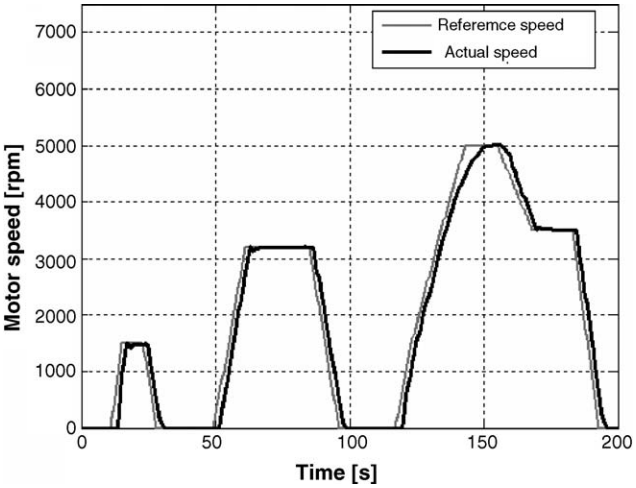

Fig. 5. European driving cycle R40.

and/or batteries during the cycle. The first experiment was carried out utilizing the fuel-cell system as a power-levelling source, while entrusting the task of providing peak power to the storage system. The value of power fixed at the dc–dc converter output corresponded to the average power of the R40 cycle (280 W).

The power distribution between FCS+ converter, engine and battery pack versus cycle length is reported in Fig. 6. The battery power curve shows that the storage system compensates for the difference between the electric drive requirements and the power provided by the feel-cell system (in Fig. 6, negative values for battery power indicate that energy is entering the storage system). The energy flowing from the battery permits the peak engine power to be achieved, while during the regenerative braking, when the motor operates as generator, the battery power drops to negative values, which indicate a partial recovery of energy.

The behaviour of battery power affects its state-of-charge (SoC) during the cycle, as shown in Fig. 7, but SoC evalua-

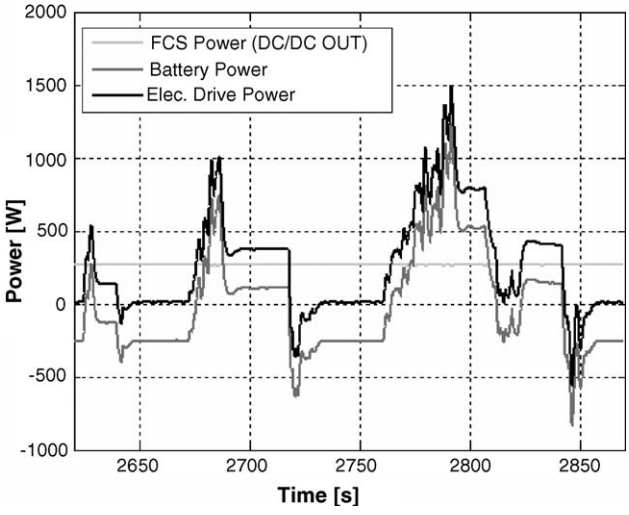

Fig. 6. Experimental results obtained on fuel-cell powertrain in a load-levelling configuration and operating under the R40 driving cycle (FCS power = average cycle power): battery, input electric drive and output dc–dc converter powers vs. cycle length.

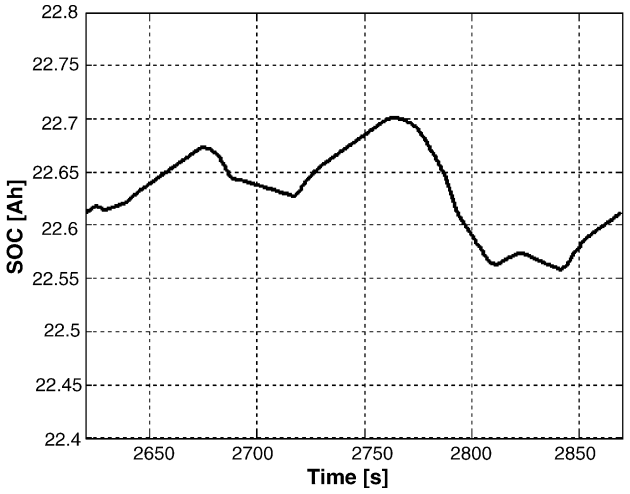

Fig. 7. Battery state-of-charge (SoC) vs. cycle length during experiment of Fig. 6.

tion requires some preliminary considerations of battery efficiency. The electrochemical efficiency of a storage battery is η_{batt} defined as ratio between the integral of the instantaneous current during a discharge and the integral during a charge, in view that the status of the battery before and after the calculation is the same:

$$\eta_{batt} = \frac{\int_0^{t_d} I_d \, dt}{\int_0^{t_c} I_c \, dt}$$

where I_d, and I_c are the battery current during the discharge and the charge periods, respectively, t_d and t_c are the lengths of the two corresponding periods. The determination of this efficiency for a specific type of battery, with reference to a particular driving cycle, requires experimental evaluation of the battery SoC, which is based on specific tests that are beyond the scope of this paper [9]. For the lead–acid batteries used in the present work, it has been experimentally verified that very low energy losses can be detected if charge and discharge operations are very fast. In particular, in short cycles of charge and discharge (about 30 mim) an energy efficiency higher than 92% has been obtained [10]. If a value of 100% for the battery energy efficiency is assumed, it is possible to define the battery state-of-charge as:

$$SOC(t) = SOC^{\circ} + \int_{t^{\circ}}^{t} I_{Batt}(t) dt \quad (3)$$

where SoC° is the known battery state-of-charge at time t°; I_{batt} is the current exchanged by the battery. This definition is utilized in this paper to calculate instantaneously the battery SoC during the driving cycles, starting from experimental measurements of the battery current. In order to verify the hypothesis of 100% for battery efficiency, a specific experimental procedure was realized. In particular, three consecutive cycles of charging and discharging were effected on a new battery pack using the experimental conditions specified by the maker to avoid energy losses. The first cycle was used to verify the actual battery capacity, during the second cycle the battery was charged to its maximum SoC, followed by discharge to 50%. Then a sequence of 100 cycles of the type shown in Fig. 6 was carried out (corresponding to 130 km). After this sequence, the battery pack was completely discharged. Finally, the energy capacity of the battery pack was again verified by a third cycle of charging and discharging according to the manufacturer specifications. This procedure showed that the battery experienced only a negligible loss in energy during the sequence of 100 cycles. On this hypothesis the SOC calculated according Eq. (3) is reported in Fig. 7, with reference to the cycle of Fig. 6. The maximum and minimum peaks of SoC correspond to the point of intersection between the FCS and electric drive power curves, i.e., when the engine begins to take energy from the battery during acceleration or batteries are recharged by the FCS during deceleration. The additional contribution to battery recharging comes from the regenerative braking. The discharging phases correspond to the energy requirements of the electric drive.

In order to achieve a complete evaluation of the efficiency of the powertrain and its components, experimental determination of the efficiencies of the converter (η_{DC}) and the electrical drive (η_{ED}) was performed. Both were calculated as the ratio between the outlet and the inlet power of the devices, i.e.,

$$\eta_{DC} = \frac{P_{OUT_{DC}}}{P_{IN_{DC}}} \quad (4)$$

$$\eta_{ED} = \frac{P_{OUT_{ED}}}{P_{IN_{ED}}} \quad (5)$$

The total efficiency of the powertrain on the driving cycle was determined using Eq. (6) with the assumption of a battery efficiency of 100% and taking back the final SoC to the initial level:

$$\eta_{PT} = \eta_{FCS}\eta_{DC}\eta_{ED} \quad (6)$$

The amounts of energy involved in the experiments of Figs. 6–7 were calculated by numerical integration during current and voltage acquisition. These values and the correlated efficiency calculations are reported in Tables 2 and 3, whose symbols have the following meanings:

$$E_{Stack} = \int_{t_1}^{t_2} P_{Stack} \, dt \qquad E_{FCS} = \int_{t_1}^{t_2} P_{IN_{DC}} \, dt$$

$$E_{DC} = \int_{t_1}^{t_2} P_{OUT_{DC}} \, dt$$

Table 2
Energy flow measurements inside fuel-cell powertrain during R40 cycle in load-levelling configuration with FCS power = average cycle power

	Wh
E_{H_2}	44.8
E_{stack}	28.0
E_{FCS}	22.5
E_{DC}	18.0
E_{ED}	17.9
E_{load}	13.4
E_{batt}	−0.4
E_{batt} IN	−10.1
E_{batt} OUT	+9.6
$E_{breaking\ regenerative}$	−1.2

Table 3
Efficiency calculations during R40 cycle in load-levelling configuration with FCS power = average cycle power

	%
η_{FCS}	50
η_{DC}	80
η_{ED}	75
η_{PT}	30

$$E_{ED} = \int_{t_1}^{t_2} P_{IN_{ED}}\,dt \qquad E_{batt} = \int_{t_1}^{t_2} V_{batt} I_{Batt}\,dt$$

$$E_{Load} = \int_{t_1}^{t_2} T_m \omega_m\,dt$$

$$E_{H_2} = \frac{1}{\eta_{utill}} \int_{t_1}^{t_2} M_{H_2} n_{cells} I \frac{\Delta H_f}{2F} dt = \int_{t_1}^{t_2} P_{H_2}\,dt$$

where V_{batt}, battery voltage; I_{batt}, battery current; T_m, brake torque; ω_m, engine speed; M_{H_2}, hydrogen molecular weight; n_{cells}, cell number; I, stack current.

E_{load} is the energy provided by the engine during the overall test procedure, while E_{H_2} is the energy coming from hydrogen and E_{batt} is the net energy exchanged by the battery pack during the cycle.

Starting from the energy associated with the fuel (45 Wh) entering the propulsion system, the energy losses due to the different components can be calculated. The fuel cells with their auxiliary components introduce a diminution of usable energy of about 50%, while minor losses are due to the electrical devices, such as the converter and engine, whose efficiency are 80 and 75%, respectively. The energy recovery due to regenerative braking is 1.2 Wh, which corresponds to about 7% of the energy entering the electric drive. The mechanical energy available for the vehicle is 13 Wh, which implies a total powertrain efficiency of about 30%. The data in Table 2 shows that a significant amount of energy passes through the storage system during the cycle (about 22% of the fuel energy). This confirms the essential role of batteries in following the dynamics of the load-levelled procedure.

Another possible working strategy for a propulsion system based on fuel cells is the load-following procedure, which allows the storage system to be minimized. In this case, the batteries on the vehicle can have the minimum capacity necessary to feed the vehicle auxiliaries and permit energy economy during regenerative braking. In a load-following configuration, the power at the converter output has to be controlled in order to supply the electric drive with all the power that is instantaneously required during the cycle. As the experimental apparatus used in this studies comprises a fuel-cell system with a power comparable with that of the engine, it was possible to perform experiments using this procedure. The power distribution between the FCS+ converter, engine and battery pack versus cycle length is reported in Fig. 8, while the powers associated with fuel, stack, and FCS are shown in Fig. 9. The limited contribution of batteries is evident from Fig. 8, in fact their power peaks are always under 500 W.

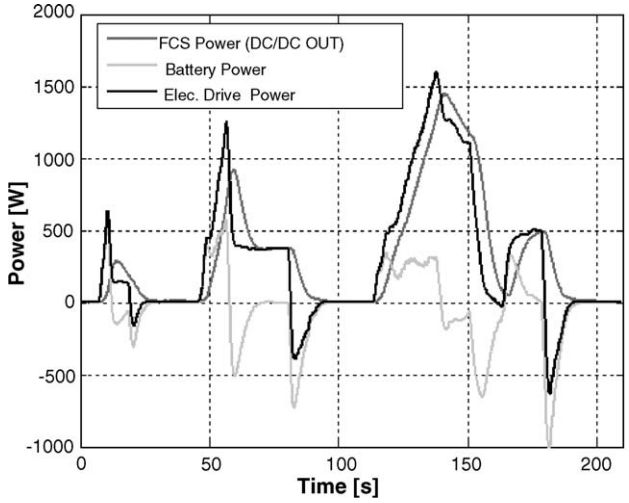

Fig. 8. Experimental results obtained on fuel-cell powertrain in load-following configuration and operating under the R40 driving cycle (FCS power = engine power): battery, input electric drive and output dc–dc converter powers vs. cycle length.

Furthermore, the storage system permits the regenerative braking in a similar whenever to the load-levelling procedure, and contributes to the dynamics at the start-up of acceleration phases of the cycle, which compensates for the delay of FCS intervention. The power curve detected at the converter output shows a satisfactory dynamic behaviour during all the R40 cycle, in particular the power peaks required by the engine are almost completely satisfied by the energy provided by the FCS through the converter. Stack and FCS dynamics are confirmed by the results of Fig. 9, from which indications of energy losses from fuel to converter inlet can also be derived.

The state-of-charge of the batteries during the load-following test is given in Fig. 10. The small variation in SoC during the R40 cycle confirms that a limited amount of energy pass through the storage system during the test. From comparison of the strongest variations in the SoC curves obtained with the two procedures (Figs. 7 and 10), it can be concluded that a battery capacity at

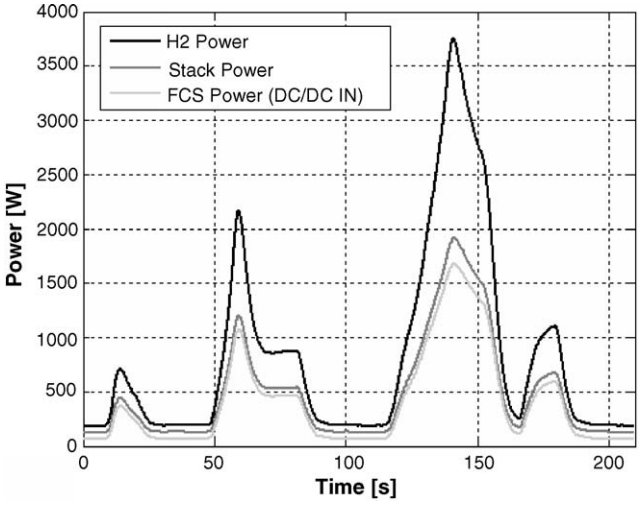

Fig. 9. Hydrogen, stack and FCS power vs. cycle length during experiment of Fig. 8.

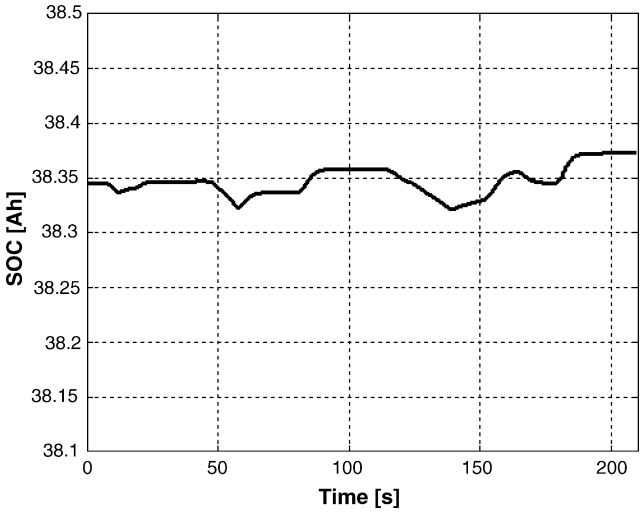

Fig. 10. Battery state-of-charge (SoC) vs. cycle length during experiment of Fig. 8.

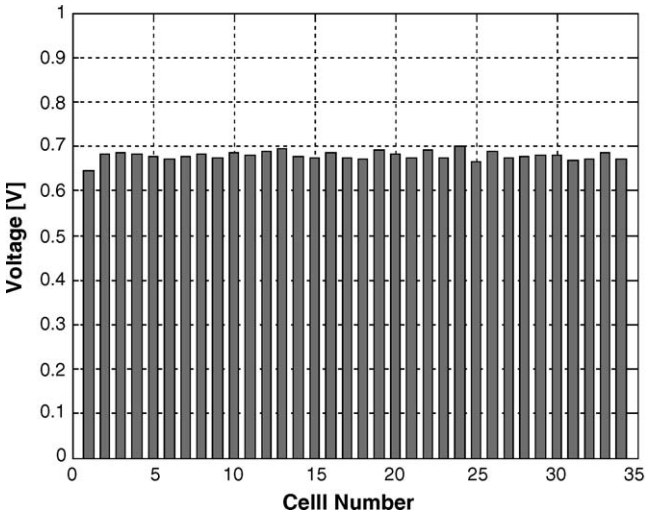

Fig. 12. Individual cell voltage at stack maximum power during the experiment of Fig. 8.

least three times lower could be adopted in the load following test.

The dynamic behaviour and performance of the FCS during the load-following test can be analysed by monitoring the stoichiometric ratio between air and fuel fed to the stack as function of cycle length. This ratio is defined as $R = R_{eff}/R_{stoich}$, where R_{eff} is the ratio between the air and hydrogen flow rates used in the experiments, while R_{stoich} is the same ratio as required by the stoichiometric equation of hydrogen oxidation. The optimum in value for R for a PEMFC ranges between 2 and 6 as function of load, and cannot drop under 1.8 in order to guarantee sufficient partial pressure of oxygen at the cathode side. During the fast acceleration phases of the R40 cycle this ratio falls below 2 for few seconds (see Fig. 11), due to the slight delay if the air compressor response with respect to power demand from the engine. In order to analyze the stack behaviour under these high load conditions the individual cell voltages were monitored, as shown in Fig. 12 in which the voltage are referred to the maximum power reached by the stack during the R40 cycle. Very good uniformity is obtained with voltage oscillations lower than 2% of the average voltage value.

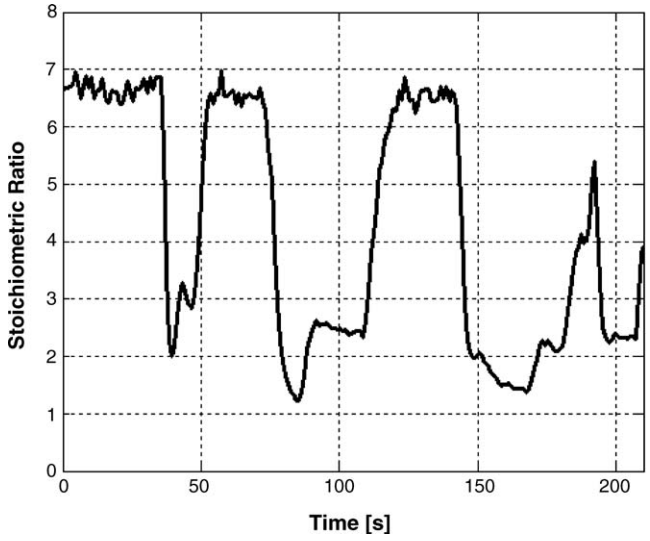

Fig. 11. Stack stoichiometric ratio vs. cycle length during experiment of Fig. 8.

The energy and efficiency calculations for the load-following test are reported in Tables 4 and 5. The energy losses due to the fuel-cell system are comparable with those detected during the load-levelling test, in fact the system efficiency (Table 5) is only slightly inferior to the corresponding value reported in Table 3 (48% versus 50%). The efficiencies of the converter and engine are equal to that of load-levelling test (80 and 75%, respectively). On the other hand the energy recovery due to the regenerative braking is 1.6 Wh, which corresponds to about 10% of the energy the electric drive (Table 4). The total powertrain efficiency is

Table 4
Energy flow measurements inside fuel-cell powertrain during R40 cycle m load-following configuration with FCS power = engine power

	Wh
E_{H_2}	48.5
E_{stack}	28.3
E_{FCS}	23.3
E_{DC}	18.5
E_{ED}	16.7
E_{load}	12.5
E_{batt}	−1.6
E_{batt}, IN	−5.5
E_{batt} OUT	+3.9
$E_{braking\ regenerative}$	−1.6

Table 5
Efficiency calculations during R40 cycle in load-following configuration with FCS power = engine power

	%
η_{FCS}	48
η_{DC}	80
η_{ED}	75
η_{PT}	29

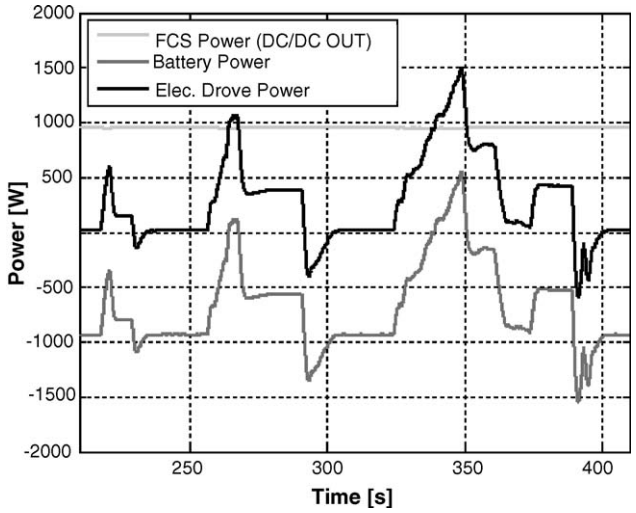

Fig. 13. Experimental results obtained on fuel-cell powertrain in load-levelling configuration and operating under the R40 driving cycle (FCS power at maximum FCS efficiency): battery, input electric drive and output dc–dc converter powers vs. cycle length.

29%. The data in Table 4 also indicate that a minimum amount of energy passes through the storage system during the cycle (about 8% of the fuel energy). This confirms the possibility of reducing the on-board battery capacity in the load- following configuration.

The results shown above were obtained using energy-management strategies based on the control of stack power during the cycle, while the following test was undertaken by controlling the battery SoC. In particular, the SoC was left free to range between two pre-fixed values, while FCS power was maintained constant at the value corresponding to is maximum efficiency (1000 W, as shown in Fig. 4). The results of this experiment are reported in Figs. 13 and 14. The storage system was charged using the R40 cycle (Fig. 13), which resulted in increase of SoC from 31.55 to 32.27 Ah (Fig. 14). The energy

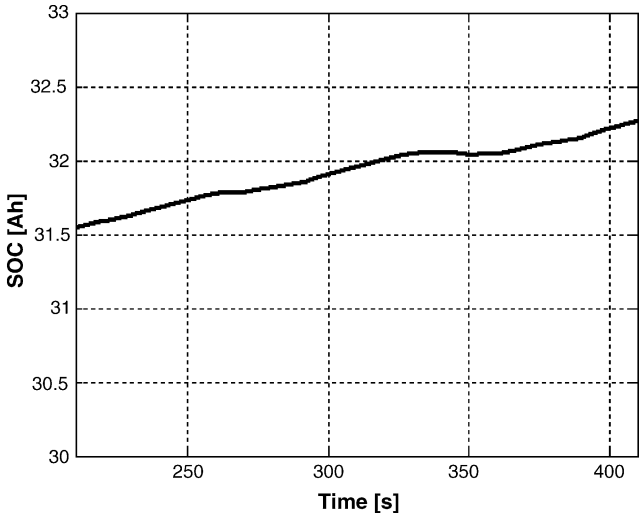

Fig. 14. Battery state-of-charge (SoC) vs. cycle length during experiment of Fig. 13.

Table 6
Energy flow measurements inside fuel-cell powertrain during R40 cycle in load-levelling configuration with FCS power at maximum FCS efficiency

	Wh
E_{H_2}	120.1
E_{stack}	68.4
E_{FCS}	60.5
E_{DC}	52.8
E_{ED}	15.1
E_{load}	11.3
E_{batt}	−37.7
E_{batt} IN	−38.7
E_{batt} OUT	+1.0
$E_{breaking\ regenerative}$	−1.4

and efficiency calculations for this experiment are reported in Tables 6 and 7. This found that the FCS efficiency (51%) is slightly higher with respect to that of the previous experiments. The electric drive efficiency remains unchanged (75%), but the converter gives a higher efficiency (87%) as it operates inside its optimum power range. Recovery of about 10% of the energy entering the engine is also observed. As a consequence, the total efficiency of the powertrain (η_{PT}) is 33%. It is necessary, however, to observe that in this control strategy a higher battery capacity has to be used with respect to the load-following procedures. In addition, the FCS has to be shut down during battery discharging at a frequency that depends on the storage system capacity.

In order to analyse the energy losses associated with the start-up phases of the FCS, the following experiments were carried out. In particular, some start-up tests were undertaken two initial stack temperatures (15 and 30 °C), and for each temperature two power accelerations were used up to 1200 W stack power (20 and 200 W s^{-1}). After each acceleration, the system was left in steady-state condition until a stack temperature of 45 °C was reached. The stack and FCS efficiencies are plotted versus time together with the stack temperature starting from 15 °C in Figs. 15 and 16. The selected final stack temperature is reached in about 10 min with both power accelerations, while the stack efficiency achieves a minimum value (at 1200 W) of about 0.53 at the end of both acceleration ramps. When the stack temperature reaches 45 °C, the efficiency increased up to 0.59, and when power reaches its set maximum value (1200 W) the FCS efficiency increases from 0.45 to 0.50 in both tests. It is possible to deference from Figs. 15 and 16 the energy losses due to the warm-up period of 600 s; they are about 5% of the FCS steady state maximum efficiency. Variation in the power accel-

Table 7
Efficiency calculations during R40 cycle in load-levelling configuration with FCS power at maximum FCS efficiency

	%
η_{FCS}	51
η_{DC}	87
η_{ED}	75
η_{PT}	33

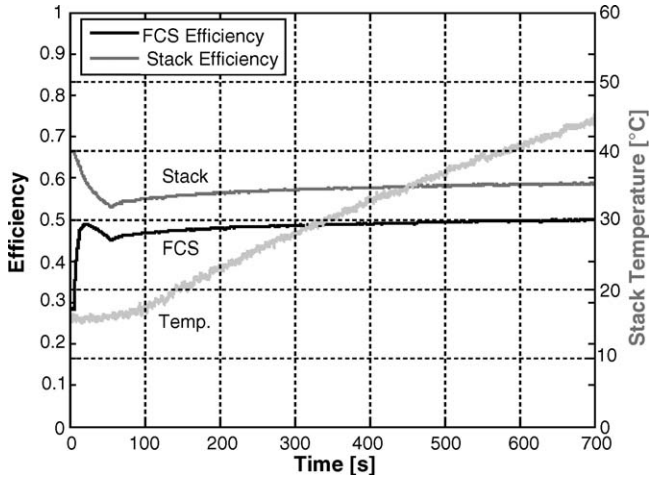

Fig. 15. FCS warm up from 15 to 45 °C, with 20 W s^{-1} up to 1.2 kW stack power. FCS efficiency, stack efficiency and temperature vs. time.

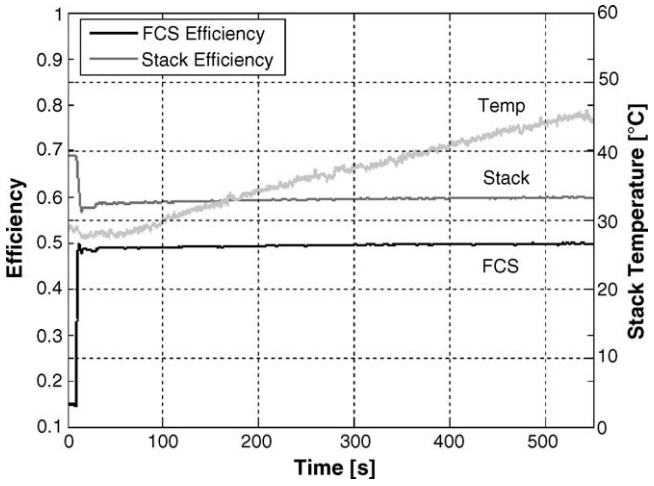

Fig. 17. FCS warm up from 30 to 45 °C, with 200 W s^{-1} up to 1.2 kW stack power. FCS efficiency, stack efficiency and temperature vs. time.

eration between 20 and 200 W s^{-1} does not significantly affect these energy losses. The start-up behaviour was also verified with 30 °C as the starting temperature. The results obtained at 20 W s^{-1} are given in Fig. 17, from which an energy loss during warm-up of about 2% is calculated. If any energy losses due to frequent start-up are taken into account, the total powertrain efficiency for the last control strategy could become comparable with that obtained with the load-levelling and load-following procedures.

The overall experimental results obtained on the fuel-cell powertrain provide some general considerations about the energy management of these propulsion systems. In particular, from Tables 3, 5 and 7, it can be observed that the total efficiency (η_{PT}) calculated on the R40 cycle is not significantly affected by the given control strategy. In fact, when the FCS and converter operate in a steady-state at their maximum efficiency conditions (see Table 7), the total efficiency, after correction for warm-up energy losses, tends towards a value of about 30

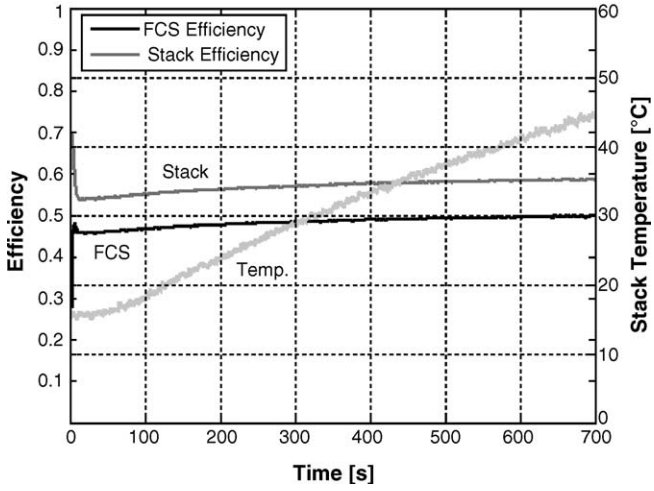

Fig. 16. FCS warm up from 15 to 45 °C, with 200 W s^{-1} up to 1.2 kW stack power. FCS efficiency, stack efficiency and temperature vs. time.

which is similar to that obtained with the other two procedures. This can be attributed to the main characteristic of a fuel-cell system, as is well demonstrated by Fig. 4, that is the negligible influence of load on FCS efficiency, which is also the main difference with respect to internal combustion engines. Only by adopting a load-following procedure on a driving cycle characterized by many and long phases of very low load, can the total efficiency because significantly lower than 30% becomes of the minor FCS efficiency. With respect of the other components of the powertrain, the effect of the converter on the total efficiency has to be first considered. In particular, this component is essential to the correct implementation of any control strategy, and should be specifically designed with respect to the application (this was not done in the present study) and carefully matched to the FCS in terms of maximum power and current On the other hand, the electric drive used in all experiments of this work is a commercial device, usually installed on electric mopeds, and its efficiency is not very high.

The main problem of electric vehicles is the requirement of large and heavy battery pack to guarantee the required driving range. On the other hand, the use of a load-following procedure in a fuel-cell powertrain permits the storage system to be strongly reduced in size with consequent benefits in terms of vehicle passenger space and energy consumption.

4. Conclusions

A fuel-cell powertrain of 2.5 kW based on a 2.5-kW PEMFC stack has been experimentally characterized in order to investigate the effect of different energy-management strategies on the performance and efficiency of single sub-systems and the total propulsion system. The tests have been carried out on a laboratory test bench that is able to simulate the European driving cycle R40.

The total efficiency of the powertrain over the driving cycle is about 30% for the three fuel-cell system control strategies investigated, namely steady-state, dynamic and steady state with

periodic shut-down/start-up. This behaviour is due to of the characteristic curve of the fuel-cell system efficiency versus load, which results in an efficiency of about 50% over a wide power range.

Taking into account other important factors, such as weight, size and durability of battery packs, the load-following control strategy appears to be the most suitable for fuel-cell vehicles in terms of fuel consumption. This is because it minimizes the on- board storage system, whose main function would then be to recover energy during regenerative braking. In this respect the use of super-capacitors, characterized by lower capacity and higher power peaks with respect to batteries, should be also considered.

Acknowledgement

The authors gratefully acknowledge Mr. Giovanni Cantilena of Istituto Motori for his cooperation in setting up the experimental apparatus and execution of the tests.

References

[1] M.H. Frank, D.L. Wetter, D.A. Masten, A. Bosco, Society of Automotive Engineers, Technical Paper No. 2000-01-0373, 2000.
[2] G. Cacciola, V. Antonucci, S. Freni, J. Power Sources 100 (2001) 67.
[3] B.D. McNicol, D.A.J. Rand, K.R. Williams, J. Power Sources 100 (2001) 47.
[4] M. Conte, A. Iacobazzi, M. Ronchetti, R. Vellone, J. Power Sources 100 (2001) 171.
[5] H.F. Creveling, in: J.M. Norbeck, et al. (Eds.), Hydrogen Fuel for Surface Transportation, Society of Automotive Engineers, Inc., Warrendale, PA, USA, 1996, p. 133.
[6] R.J. Potter, T.R. Ralph, D. Thompsett, G.T. Burstein, G.J. Hutchings, Catal. Today 38 (1997) 393.
[7] P. Corbo, F.E. Corcione, F. Migliardini, O. Veneri, J. Power Sources 145 (2005) 610.
[8] S. Dhameja, Electric Vehicle Battery Systems, Newnes (Butterworth-Heinemann), Boston, MA, USA, 2002, p. 24.
[9] I.R. Hill, Ed.E. Andrukaitis, J. Power Sources 103 (2001) 98.
[10] G.W. Vinal, Storage Batteries, John Wiley & Sons Inc., New York, NY, USA, 1955, p. 332.